PAGEOPH, Vol. 139, No. 3/4 (1992) 0033-4553/92/040535-26$1.50 + 0.20/0

Induced Stresses due to Fluid Extraction from Axisymmetric Reservoirs

PAUL SEGALL[1]

Abstract—Earthquakes can be induced by fluid extraction, as well as by fluid injection. SEGALL (1989) proposed that poroelastic stresses are responsible for inducing earthquakes associated with fluid extraction. Here, I present methods for computing poroelastic stress changes due to fluid extraction for general axisymmetric reservoir geometries. The results of GEERTSMA (1973) for a thin disk reservoir with uniform pressure drop are recovered as a special case. Predicted surface subsidence agrees very well with measured leveling changes over the deep Lacq gas field in southwestern France. The induced stresses are finite if the reservoir pressure changes are continuous. Computed stress changes are on the order of several bars, suggesting that the preexisting stress states in regions of extraction induced seismicity are very close to frictional instability prior to production.

Key words: Induced seismicity, poroelasticity, fluid extraction.

1. Introduction

Earthquakes can be induced by injection of fluids into the earth. It is widely accepted that these earthquakes are triggered by the decrease in "effective" normal stress acting across fault surfaces that results from an increase in pore pressure (HEALY *et al.*, 1968; RALEIGH *et al.*, 1972, 1976; HSIEH and BREDEHOEFT, 1981). Since pore pressure does not alter shear stresses, it is assumed that the faults slip under the preexisting shear stress. Given this mechanical framework it has been difficult to explain the observation that seismicity and aseismic fault slip have been associated with fluid *extraction* in a number of oil and gas fields (YERKES and CASTLE, 1976). It is now well established from seismicity studies that earthquakes are occurring near oil and gas fields in Texas (PENNINGTON *et al.*, 1986; DOSER *et al.*, 1991), Alberta, Canada (WETMILLER, 1986), and at Lacq in southwestern France (GRASSO and WITTLINGER, 1990). Pore pressures in these fields have *declined* by several 10's of MPa. Since fluid extraction decreases pore pressure, the

[1] Department of Geophysics, Stanford University and U.S. Geological Survey, Menlo Park, California, U.S.A.

simple effective stress argument says that fluid extraction should increase the effective confining stress acting on potential fault surfaces, thereby inhibiting slip.

SEGALL (1989) suggested that poroelastic stresses resulting from production-generated decreases in pore pressure are responsible for earthquakes in these fields. The mechanics are quite simple. Rocks contract when fluids are removed from their pores. Pore pressures decrease much more in the permeable reservoir beds than they do in the surrounding low permeability units. This leads to a strain mismatch, with the reservoir rocks shrinking more than the surroundings, and this strain generates stress. The physics is very similar, but not identical, to thermoelastic stressing, with pore-pressure analogous to temperature.

Fluid extraction induces deformation, which may occur both seismically and aseismically. Subsidence associated with hydrocarbon production reached 9 meters at the Wilmington oil field between 1936 and 1966. Horizontal displacements were as great as 3.7 meters (YERKES and CASTLE, 1970). More recently, subsidence of 4.0 meters in the North Sea Ekofisk field (SULAK and DANIELSEN, 1988) necessitated the raising of offshore platforms at a cost of $356,700,000 (SMITH, 1988). Lesser subsidence in the Groningen field, Netherlands has resulted in comparable damage. Faulting associated with production has sheared wells and buckled pipelines (KOCH, 1933; YERKES and CASTLE, 1970). Of course, ground motions from even moderate-sized, shallow earthquakes can cause severe damage.

Previously, KOSLOFF *et al.* (1980a,b) used the finite element method and measured reservoir pressure changes to model subsidence in the Wilmington field. They found it necessary to include inelastic effects to satisfactorily match the observed subsidence. SEGALL (1985) computed the stress changes on the 1983 Coalinga fault surface due to extraction from overlying oil fields. In part, because the earthquake was so much deeper than the oil and gas fields, the calculated stresses were found to be only slightly greater than tidal stresses, suggesting that the 1983 earthquake was not induced.

This paper extends previously analytical studies and presents solutions for stress and deformation fields induced by fluid extraction for general axisymmetric geometries. In doing so we build on the work of GEERTSMA (1973) who derived the stress and displacement fields for a disk-shaped reservoir. I follow Geertsma and assume that the pressure distribution within the reservoir is given as a function of space and time from field data and/or reservoir simulations. The Green's functions for a radial pressure source (or sink) are derived here. With these Green's functions it is possible to model flat reservoirs with arbitrary radial pressure distributions. It is also possible to model axisymmetric dome shaped reservoirs.

2. Theory

The constitutive equations for a linear poroelastic medium, assuming material isotropy, are

$$2\mu\epsilon_{ij} = \sigma_{ij} - \frac{\nu}{1+\nu}\sigma_{kk}\delta_{ij} + \frac{(1-2\nu)\alpha}{1+\nu}p\delta_{ij} \tag{1}$$

and

$$\Delta m = \frac{(1-2\nu)\alpha\rho_0}{2\mu(1+\nu)}\left[\sigma_{kk} + \frac{3}{B}p\right] \tag{2}$$

(BIOT, 1941; RICE and CLEARY, 1976). Equation (1) relates the strain ϵ_{ij} to the stress acting on the material element σ_{ij} and the pore pressure p. Equation (2) relates the change in fluid mass per unit volume (Δm) to the mean normal stress σ_{kk} and pore pressure p. In (2) $m = \rho v$, where ρ is the fluid density (ρ_0 in the reference state), and v the fluid volume fraction.

For isotropic poroelastic media there are four material constants. In the form of equations (1) and (2), they are the shear modulus μ, Poisson's ratio ν of classical elasticity, Skempton's coefficient B, and the Biot pore-pressure coefficient α. According to simple micromechanical models, α is related to the bulk moduli of the saturated rock (K) and the grains in the rock (K_s) by $\alpha = 1 - K/K_s$ (NUR and BYERLEE, 1971). Thus, α is expected to be an increasing function of porosity; with vanishing porosity $\alpha \to 0$, whereas with increasing porosity $\alpha \to 1$. Skempton's coefficient B is the ratio of induced pore pressure to confining stress under "undrained" (no flow) conditions. Note that for $\Delta m = 0$ equation (2) gives $p = -B\sigma_{kk}/3$.

The solid volume strain can be related to changes in mean stress and pore pressure by taking the contraction of (1)

$$\epsilon_{kk} = \frac{\sigma_{kk}}{3K} + \frac{\alpha p}{K}. \tag{3}$$

Equation (3) reveals that if rock is free from constraints ($\sigma_{kk} = 0$) it will tend to contract by an amount $\alpha p/K$ when subject to a decrease in pore pressure ($p < 0$). On the other hand if the reservoir is perfectly constrained ($\epsilon_{kk} = 0$), it will be driven into tension $\sigma_{kk} = -3\alpha p$ by a reduction in pore pressure. In reality, the rocks surrounding a reservoir provide an incomplete constraint so that the reservoir shrinks (by less than $\alpha p/K$) and is put under tension. The contraction of the reservoir stresses the surrounding rocks. The precise magnitude and distribution of these stresses can be calculated if the pore-pressure change in the reservoir is known.

The equilibrium equations are

$$\frac{\partial \sigma_{ij}}{\partial x_j} + f_i = 0 \tag{4}$$

where f_i are body forces. The equilibrium equations can be cast in terms of displacements and pore pressure. The kinematic relations between strain and displacement,

$$\epsilon_{ij} = \tfrac{1}{2}\left(\frac{\partial u_i}{\partial x_j} + \frac{\partial u_j}{\partial x_i}\right) \tag{5}$$

together with equation (1) allow us to write the stress in terms of the pore pressure and displacements as,

$$\sigma_{ij} = \mu\left(\frac{\partial u_i}{\partial x_j} + \frac{\partial u_j}{\partial x_i}\right) + \frac{2\mu\nu}{1-2\nu}\frac{\partial u_k}{\partial x_k}\delta_{ij} - \alpha p \delta_{ij}. \tag{6}$$

Substituting this expression into the equilibrium equations (4) yields,

$$\mu \nabla^2 u_i + \frac{\mu}{(1-2\nu)}\frac{\partial^2 u_j}{\partial x_i \partial x_j} - \alpha \frac{\partial p}{\partial x_i} + f_i = 0. \tag{7}$$

An additional field equation governing the distribution of pore fluid is obtained by combining Darcy's law with conservation of fluid mass. Darcy's law for isotropic media, ignoring body forces acting on the fluid, is

$$q_i = -\frac{\rho_0 \kappa}{\eta}\frac{\partial p}{\partial x_i} \tag{8}$$

where q_i is fluid mass flux, κ is permeability, with dimensions of area, and η is fluid viscosity. Conservation of fluid mass requires

$$\frac{\partial q_i}{\partial x_i} + \frac{\partial m}{\partial t} = 0. \tag{9}$$

Combining equations (8) and (9) with a compatibility condition

$$\nabla^2 \sigma_{kk} + \frac{2\alpha(1-2\nu)}{(1-\nu)}\nabla^2 p = 0 \tag{10}$$

(RICE and CLEARY, 1976) yields a diffusion equation in fluid mass content

$$c\nabla^2 m = \frac{\partial m}{\partial t} \tag{11}$$

(BIOT, 1941), where the hydraulic diffusivity c is given by

$$c = \frac{\kappa}{\eta}\frac{2\mu(1-\nu)}{(1-2\nu)}\left[\frac{B(1+\nu)}{3\alpha(1-\nu) - 2B\alpha^2(1-2\nu)}\right]. \tag{12}$$

As noted by RICE and CLEARY (1976), (11) is equivalent to a diffusion equation in a linear combination of pore pressure and mean normal stress.

$$c\nabla^2\left(\sigma_{kk}+\frac{3}{B}p\right)=\frac{\partial}{\partial t}\left(\sigma_{kk}+\frac{3}{B}p\right). \tag{13}$$

In general, the deformation and pore-pressure fields are coupled through the equilibrium equations for the solid and the diffusion equation governing pore fluid flow. It is beyond the scope of the present work to attempt to *solve* for the pore-pressure distribution $p(\mathbf{x}, t)$ within an oil or gas field. Rather, we will take $p(\mathbf{x}, t)$ within the reservoir to be given from field measurements and reservoir simulations. In many practical applications the hydraulic diffusivities of the rocks surrounding the reservoir are sufficiently low that the deformation outside the reservoir is undrained. In this case, one can compute the stress from (6) assuming undrained deformation outside the reservoir. Given $p(\mathbf{x}, t)$ we can solve for the stress and displacements directly as shown below. Uncoupling the pore-pressure and deformation fields in this manner makes the present poroelastic problem completely analogous to (uncoupled) thermoelasticity and allows us to make use of well-known methods in this field.

2.1 Method of Solution

As a first step I show that the poroelastic displacements are generated by a distribution of centers of dilatation with magnitude proportional to $\alpha p(\mathbf{x})$. This is physically reasonable as (3) shows that $\alpha p(\mathbf{x})$ governs the volumetric strain in the reservoir.

First note that $-\alpha(\partial p/\partial x_i)$ enters the equilibrium equations (7) equivalent to body forces f_i. Thus if $g_i^k(\mathbf{x}, \zeta)$ represents the elastostatic Green's function, that is, the displacement in the i-direction at $\mathbf{x}$ due to a body force in the k-direction at ζ, i.e.,

$$\mu u_i(\mathbf{x}) = \int_V f_k(\zeta) g_i^k(\mathbf{x}, \zeta)\, dV_\zeta \tag{14}$$

then gradients in pore pressure induce displacements

$$\mu u_i(\mathbf{x}) = -\alpha \int_V \frac{\partial p}{\partial \zeta_k} g_i^k(\mathbf{x}, \zeta)\, dV_\zeta. \tag{15}$$

Integrating by parts, assuming that we are considering localized pore pressure disturbances, that is $p(\zeta \to \infty) = 0$ yields,

$$\mu u_i(\mathbf{x}) = \alpha \int_V p(\zeta) \frac{\partial g_i^k(\mathbf{x}, \zeta)}{\partial \zeta_k}\, dV_\zeta. \tag{16}$$

Note that $\partial g_i^k(\mathbf{x}, \zeta)/\partial \zeta_k$ is a sum of force couples acting along three orthogonal axes, that is, a center of dilatation. If we define the displacement Green's function for a center of dilatation as

$$g_i(\mathbf{x}, \zeta) \equiv \frac{\partial g_i^k(\mathbf{x}, \zeta)}{\partial \zeta_k} \tag{17}$$

(LOVE, 1944) then it follows that,

$$u_i(\mathbf{x}, t) = \frac{\alpha}{\mu} \int_V p(\zeta, t) g_i(\mathbf{x}, \zeta)\, dV_\zeta \tag{18}$$

and

$$\sigma_{ij}(\mathbf{x}, t) = \alpha \left[\int_V p(\zeta, t) G_{ij}(\mathbf{x}, \zeta)\, dV_\zeta - p(\mathbf{x}, t)\delta_{ij} \right] \tag{19}$$

where the stress Green's functions are obtained from the displacements by

$$G_{ij} = \frac{\partial g_i}{\partial x_j} + \frac{\partial g_j}{\partial x_i} + \frac{2\nu}{1 - 2\nu} \frac{\partial g_k}{\partial x_k} \delta_{ij}. \tag{20}$$

2.2 Displacement Potential

In this section we compute the appropriate Green's functions. GOODIER (1937) showed that the thermoelastic equilibrium equations could be reduced to Poisson's equation by introducing a displacement potential Φ such that

$$\frac{\partial \Phi}{\partial x_i} = u_i. \tag{21}$$

Introducing Φ into the equilibrium equations (4), neglecting body forces, and integrating yields

$$\nabla^2 \Phi(\mathbf{x}) = \frac{\alpha(1 - 2\nu)}{2\mu(1 - \nu)} p(\mathbf{x}). \tag{22}$$

MINDLIN and CHENG (1950) showed that Goodier's method can easily be extended to a homogenous half-space. Specifically, they show that for the half-space

$$\mathbf{u} = \nabla \Phi_1 + \nabla_2 \Phi_2 \tag{23}$$

where Φ_1 is the potential defined in (21), and Φ_2 is the "image potential" found by replacing the source coordinates $(\zeta_1, \zeta_2, \zeta_3)$ with the image point $(\zeta_1, \zeta_2, -\zeta_3)$. The operator ∇_2 is defined as

$$\nabla_2 = (3 - 4\nu)\nabla + 2\nabla z \frac{\partial}{\partial z} - 4(1 - \nu)\hat{\mathbf{e}}_z \nabla^2 z \tag{24}$$

where $\hat{\mathbf{e}}_z$ is the unit vector in the z direction. The operator ∇_2 corresponds to the superposition of an image center of dilatation, a double force, and a doublet sufficient to remove the tractions acting on $z = 0$.

The problem thus reduces to finding the appropriate solution to Poisson's equation. I will restrict attention to axisymmetric configurations, that is no displacement in the circumferential direction. The Green's function for the radially symmetric case, corresponding to a ring of dilatation at radius ρ and depth d can be found following NOWACKI (1962). Given this result we find the solution for an arbitrary radial pressure distribution as:

$$u_i(r, z) = \frac{\alpha}{\mu} \int_0^\infty \int_0^\infty p(\rho, d) g_i(r, z; \rho, d)\, d\rho\, dd. \tag{25}$$

On the way we recover the solution of GEERTSMA (1973) for a uniform pressure change in a thin flat disk.

To determine the radial Green's function we seek a solution to

$$\nabla^2 \Phi(r, z) = \frac{\alpha(1 - 2\nu)}{2\mu(1 - \nu)} \delta(r - \rho)\delta(z - d). \tag{26}$$

Expanding the right-hand side of (26) in appropriate orthogonal functions (e.g., JACKSON, 1962),

$$\delta(z - d) = \frac{1}{\pi} \int_0^\infty \cos \gamma(z - d)\, d\gamma \tag{27}$$

$$\delta(r - \rho) = \rho \int_0^\infty k J_0(kr) J_0(k\rho)\, dk \tag{28}$$

and the potential $\Phi(r, z)$ as

$$\Phi(r, z) = \int_0^\infty A(k) J_0(kr)\, dk \int_0^\infty \cos(\gamma z)\, d\gamma \tag{29}$$

and substituting equation (29) into

$$\nabla^2 \Phi(r, z) = \frac{\partial^2 \Phi}{\partial r^2} + \frac{1}{r} \frac{\partial \Phi}{\partial r} + \frac{\partial^2 \Phi}{\partial z^2} \tag{30}$$

leads to

$$\nabla^2 \Phi(r, z) = -\int_0^\infty \int_0^\infty A(k) J_0(kr)(k^2 + \gamma^2) \cos(\gamma z)\, d\gamma\, dk \tag{31}$$

where we have made use of the following

$$\frac{\partial J_0(x)}{\partial x} = -J_1(x) \tag{32}$$

$$2\frac{\partial J_\nu(x)}{\partial x} = J_{\nu-1}(x) - J_{\nu+1}(x) \tag{33}$$

$$\frac{2\nu}{x} J_\nu(x) = J_{\nu-1}(x) + J_{\nu+1}(x). \tag{34}$$

Now substituting (31), (27) and (28) into (26) we find that

$$A(k)\cos(\gamma z) = -\frac{\alpha(1-2\nu)}{2\mu(1-\nu)}\frac{\rho}{\pi} kJ_0(k\rho)(k^2+\gamma^2)^{-1}\cos\gamma(z-d) \tag{35}$$

so that

$$\Phi(r,z) = -\frac{\alpha(1-2\nu)}{2\mu(1-\nu)}\frac{\rho}{\pi}\int_0^\infty\int_0^\infty \frac{kJ_0(kr)J_0(k\rho)\cos\gamma(z-d)}{k^2+\gamma^2}\,d\gamma\,dk. \tag{36}$$

This is further simplified by noting that for $m \geq 0$

$$\int_0^\infty \frac{\cos(mt)}{1+t^2}\,dt = \frac{\pi}{2}e^{-m} \tag{37}$$

which leads to

$$\Phi_1(r,z) = -\frac{\alpha(1-2\nu)}{2\mu(1-\nu)}\frac{\rho}{2}\int_0^\infty J_0(kr)J_0(k\rho)\,e^{\epsilon k(z-d)}\,dk \tag{38}$$

where $\epsilon = -1$ for $z \geq d$, and $\epsilon = 1$ for $z < d$. The image potential Φ_2 is then found simply by replacing $\epsilon k(z-d)$ with $-k(z+d)$ in the exponential.

2.3 Displacements

The displacement Green's functions are computed directly by differentiating the potential according to (23). This gives

$$g_r(r,z) = \frac{(1-2\nu)}{2(1-\nu)}\frac{\rho}{2}\int_0^\infty kJ_1(kr)J_0(k\rho)[e^{\epsilon k(z-d)} + e^{-k(z+d)}(3-4\nu-2kz)]\,dk \tag{39}$$

and

$$g_z(r,z) = -\frac{(1-2\nu)}{2(1-\nu)}\frac{\rho}{2}\int_0^\infty kJ_0(kr)J_0(k\rho)[\epsilon\, e^{\epsilon k(z-d)} + e^{-k(z+d)}(3-4\nu+2kz)]\,dk. \tag{40}$$

The displacements at the free surface $z = 0$ are

$$g_r(r, z=0) = (1-2\nu)\rho\int_0^\infty kJ_1(kr)J_0(k\rho)\,e^{-kd}\,dk \tag{41}$$

and

$$g_z(r, z=0) = -(1-2\nu)\rho \int_0^\infty k J_0(kr) J_0(k\rho)\, e^{-kd}\, dk. \tag{42}$$

EASON *et al.* (1955) give these integrals in the form of elliptic integrals. Specifically, at the free surface

$$g_r(r, z=0) = (1-2\nu)\rho \left[\frac{\kappa^3 (r^2 - \rho^2 - d^2) E(\kappa)}{8\pi r (1-\kappa^2)(\rho r)^{3/2}} + \frac{\kappa F(\kappa)}{2\pi r \sqrt{\rho r}} \right] \tag{43}$$

$$g_z(r, z=0) = -(1-2\nu)\rho \frac{d\kappa^3 E(\kappa)}{4\pi (1-\kappa^2)(\rho r)^{3/2}} \tag{44}$$

where $F(\kappa)$ and $E(\kappa)$ are the complete elliptic integrals of the first and second kind respectively, and $\kappa^2 = 4r\rho/(\rho + r)^2 + d^2$.

The vertical Green's function at the free surface is shown in Figure 1 for a source radius of 3.0 and source depth of 1.0. For a shallow source, such as this, there is a ring of uplift at the source radius. As the source deepens the uplift broadens and the amplitude decreases (Figure 2). Eventually, the ring of uplift becomes a central bulge (Figure 2). This means that one cannot distinguish the toroidal source from a point source when the depth is much greater than the source radius.

For a distributed pressure source the displacement is the convolution of the Green's function with the pressure distribution. In Figure 3 the surface vertical displacement at $r = 0$ is shown as a function of the source radius. The contribution from $\rho = 0$ is zero as a source of zero radius has no strength. The influence function increases linearly for small ρ and reaches a maximum between $\rho = 0$ and $\rho = d$.

The surface radial Green's functions are shown in Figure 4. For a shallow source the radial displacements are inward for $r < \rho$ and outward for $r > \rho$. As the source deepens the radial displacements become outward directed everywhere as is the case for the point source.

2.4 Strains

The Green's functions $\hat{\epsilon}_{ij}$ for the three normal strains are now given simply from the displacements

$$\hat{\epsilon}_{rr} = \frac{\partial g_r}{\partial r} = \frac{(1-2\nu)}{2(1-\nu)} \frac{\rho}{4} \int_0^\infty k^2 [J_0(kr) - J_2(kr)] J_0(k\rho) \times [e^{\epsilon k(z-d)} + e^{-k(z+d)}(3 - 4\nu - 2kz)]\, dk \tag{45}$$

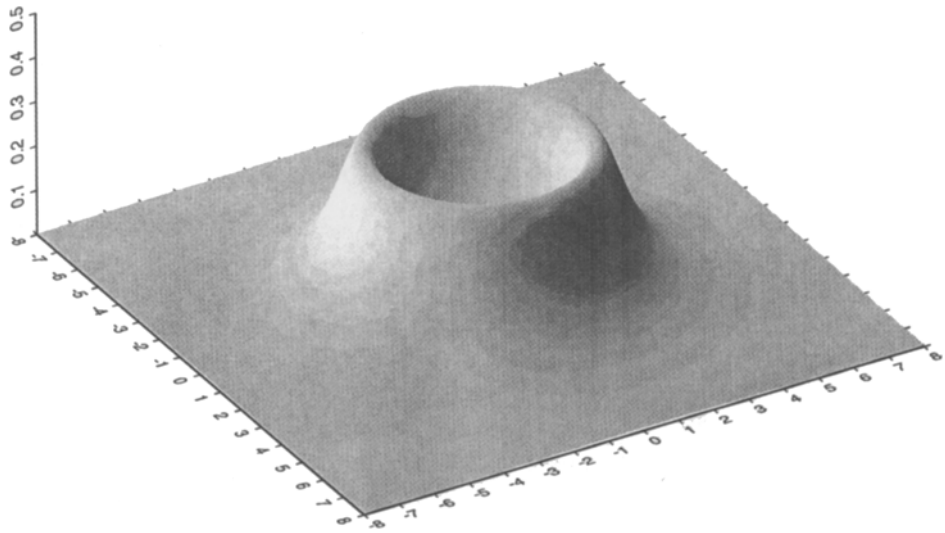

Figure 1
Vertical Green's function at the free surface. Displacement for ring pore-pressure source of magnitude p with source radius $\rho = 3.0$ and depth $d = 1.0$. Displacements are normalized by $-\alpha p(1-2\nu)/\mu$.

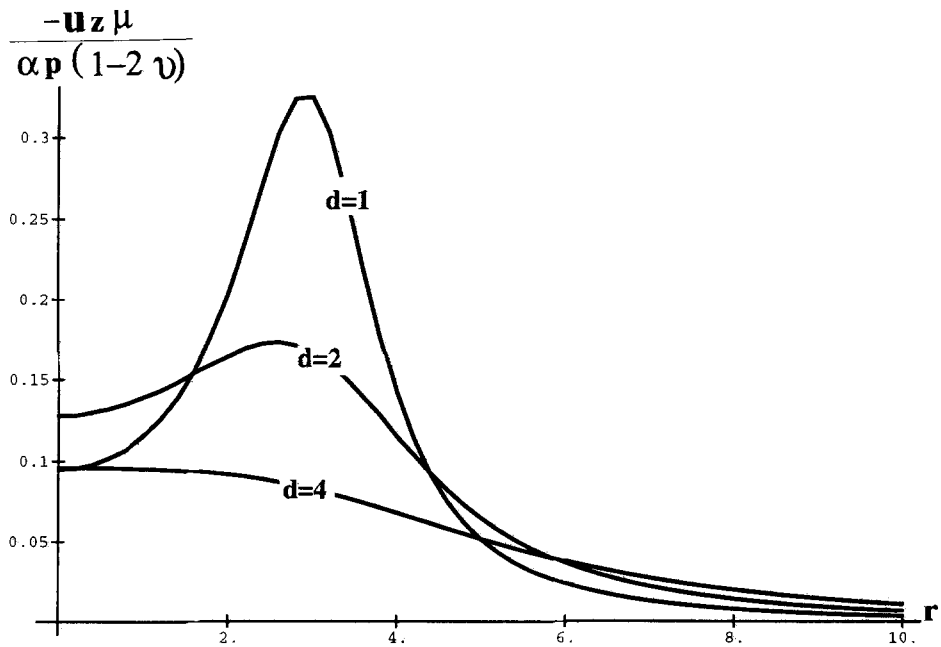

Figure 2
Vertical Green's functions at the free surface. Displacements for ring pore-pressure source of magnitude p at source radius $\rho = 3.0$ and depths $d = 1$, 2, and 4.

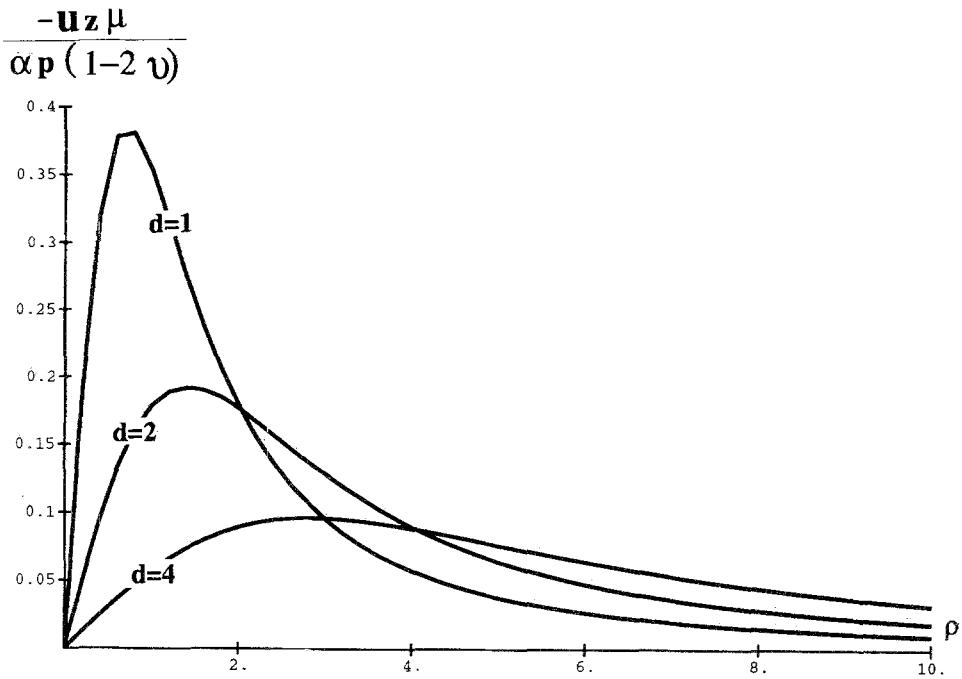

Figure 3
Vertical surface displacement at the origin ($r = 0$) as a function of the radius of the ring source ρ. Source depths $d = 1$, 2, and 4; magnitude p.

$$\hat{\epsilon}_{zz} = \frac{\partial g_z}{\partial z} = \frac{-(1-2v)}{2(1-v)} \frac{\rho}{2} \int_0^\infty k^2 J_0(kr) J_0(k\rho)[e^{ck(z-d)} - e^{-k(z+d)}(1 - 4v + 2kz)]\, dk \tag{46}$$

$$\hat{\epsilon}_{\theta\theta} = \frac{g_r}{r} = \frac{(1-2v)}{2(1-v)} \frac{\rho}{4} \int_0^\infty k^2 [J_0(kr) + J_2(kr)] J_0(k\rho) \times [e^{ck(z-d)} + e^{-k(z+d)}(3 - 4v - 2kz)]\, dk \tag{47}$$

so that the volume strain $\hat{\epsilon}_{kk} = \hat{\epsilon}_{rr} + \hat{\epsilon}_{zz} + \hat{\epsilon}_{\theta\theta}$ is given by

$$\hat{\epsilon}_{kk} = \frac{(1-2v)^2}{(1-v)} \rho \int_0^\infty k^2 e^{-k(z+d)} J_0(kr) J_0(k\rho)\, dk. \tag{48}$$

Note that, because the center of dilatation in a full space generates a pure shear, the volume strain comes only from the image source. The shear strain is

$$\hat{\epsilon}_{rz} = \tfrac{1}{2}\left(\frac{\partial g_z}{\partial r} + \frac{\partial g_r}{\partial z}\right) = \frac{(1-2v)}{2(1-v)} \frac{\rho}{2} \times \int_0^\infty k^2 J_1(kr) J_0(k\rho)[\epsilon\, e^{ck(z-d)} - e^{-k(z+d)}(1 - 2kz)]\, dk. \tag{49}$$

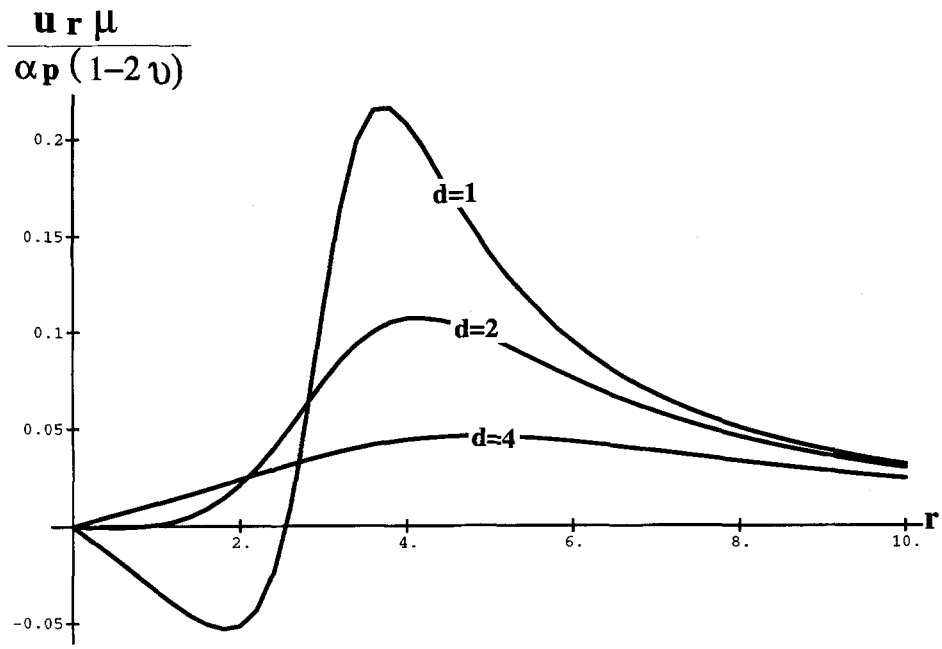

Figure 4
Radial Green's functions at the free surface. Displacements for ring pore-pressure source of magnitude p at source radius $\rho = 3.0$ and depths $d = 1$, 2, and 4.

The strains can now be written as integrals of the pressure distribution as

$$\epsilon_{ij}(r, z) = \frac{\alpha}{\mu} \int_0^\infty \int_0^\infty p(\rho, d)\hat{\epsilon}_{ij}(r, z; \rho, d)\, d\rho\, dd. \tag{50}$$

The kernels, equations (45) to (49), are all of the form

$$\hat{\epsilon}_{ij}(r, z; \rho, d) \propto \rho \int_0^\infty k^2 f_{ij}(r, z; d, k) J_0(k\rho)\, dk. \tag{51}$$

From a computational standpoint, the difficulty is that the kernels $\hat{\epsilon}_{ij}$ are hypersingular at $r = \rho$, $z = d$. This can be partially overcome by integrating by parts, with respect to ρ to reduce the order of singularity to $\propto 1/(r - \rho)$. Let us define

$$\epsilon_{ij}^{(1)} \equiv \int \hat{\epsilon}_{ij}\, d\rho \tag{52}$$

then

$$\epsilon_{ij}^{(1)} = \int \rho \int_0^\infty k^2 f_{ij}(r, z; d, k) J_0(k\rho)\, dk\, d\rho. \tag{53}$$

Interchanging the order of integration, and noting that

$$\int \rho J_0(k\rho)\, d\rho = k^{-1}\rho J_1(k\rho) \tag{54}$$

yields

$$\epsilon_{ij}^{(1)} = \rho \int_0^\infty k f_{ij}(r, z; d, k) J_1(k\rho)\, dk. \tag{55}$$

Note that $\epsilon_{ij}^{(1)}$ is the strain due to a disk of radius ρ with uniform pressure change (GEERTSMA, 1973). Thus, integrating by parts, we can write the strain as

$$\epsilon_{ij}(r, z) = -\frac{\alpha}{\mu} \int_0^\infty \int_0^\infty \frac{\partial p(\rho, d)}{\partial \rho} \epsilon_{ij}^{(1)}(r, z; \rho, d)\, d\rho\, dd. \tag{56}$$

The boundary terms vanish if the pressure change vanishes at infinity ($p(\rho = \infty) = 0$), because $\epsilon_{ij}^{(1)}(\rho = 0) = 0$. The latter must be true according to the definition (52), since this term corresponds to the strain due to a uniformly pressurized disk with zero radius.

The expressions for the $\epsilon_{ij}^{(1)}$ are simply obtained from equations (45) to (49) above by substituting $J_1(k\rho)$ for $J_0(k\rho)$ and k for k^2, and changing the sign.

By integrating by parts we have reduced but not eliminated the singularities in the strain components. Specifically, ϵ_{rr} and ϵ_{zz} behave like $1/2\pi(r-\rho)$ and $-1/2\pi(r-\rho)$ for small $(r-\rho)$, respectively. ϵ_{rz} is zero on $z = \xi$, by symmetry, but behaves like $(z-d)/2\pi(r-\rho)^2 + (z-d)^2$ for small $(r-\rho)$. The $\epsilon_{\theta\theta}$ component is nonsingular.

2.5 Stresses

From the above expressions for the strains we can simply compute the stress components from equation (20). The stresses can thus be written in the form,

$$\sigma_{ij}(r, z) = \alpha \left[\frac{(1-2\nu)}{2(1-\nu)} \int_0^\infty \int_0^\infty \frac{\partial p(\rho, d)}{\partial \rho} G_{ij}(r, z; \rho, d)\, d\rho\, dd - p\delta_{ij} \right] \tag{57}$$

where the G_{ij} are given below. I will adopt the shorthand notation of EASON *et al.* (1955) as modified by GEERTSMA (1973). Let

$$I^c(n, m; t) = \int_0^\infty J_n(k\rho) J_m(kr) k^t e^{-ck}\, dk. \tag{58}$$

Then the G_{ij} can be written as

$$\begin{aligned} G_{rr} = \frac{\rho}{2} \{ & I^{-\epsilon(z-d)}(1, 0; 1) + (3+4\nu) I^{(z+d)}(1, 0; 1) - 2z I^{(z+d)}(1, 0; 2) \\ & - I^{-\epsilon(z-d)}(1, 2; 1) - (3-4\nu) I^{(z+d)}(1, 2; 1) + 2z I^{(z+d)}(1, 2; 2) \} \end{aligned} \tag{59}$$

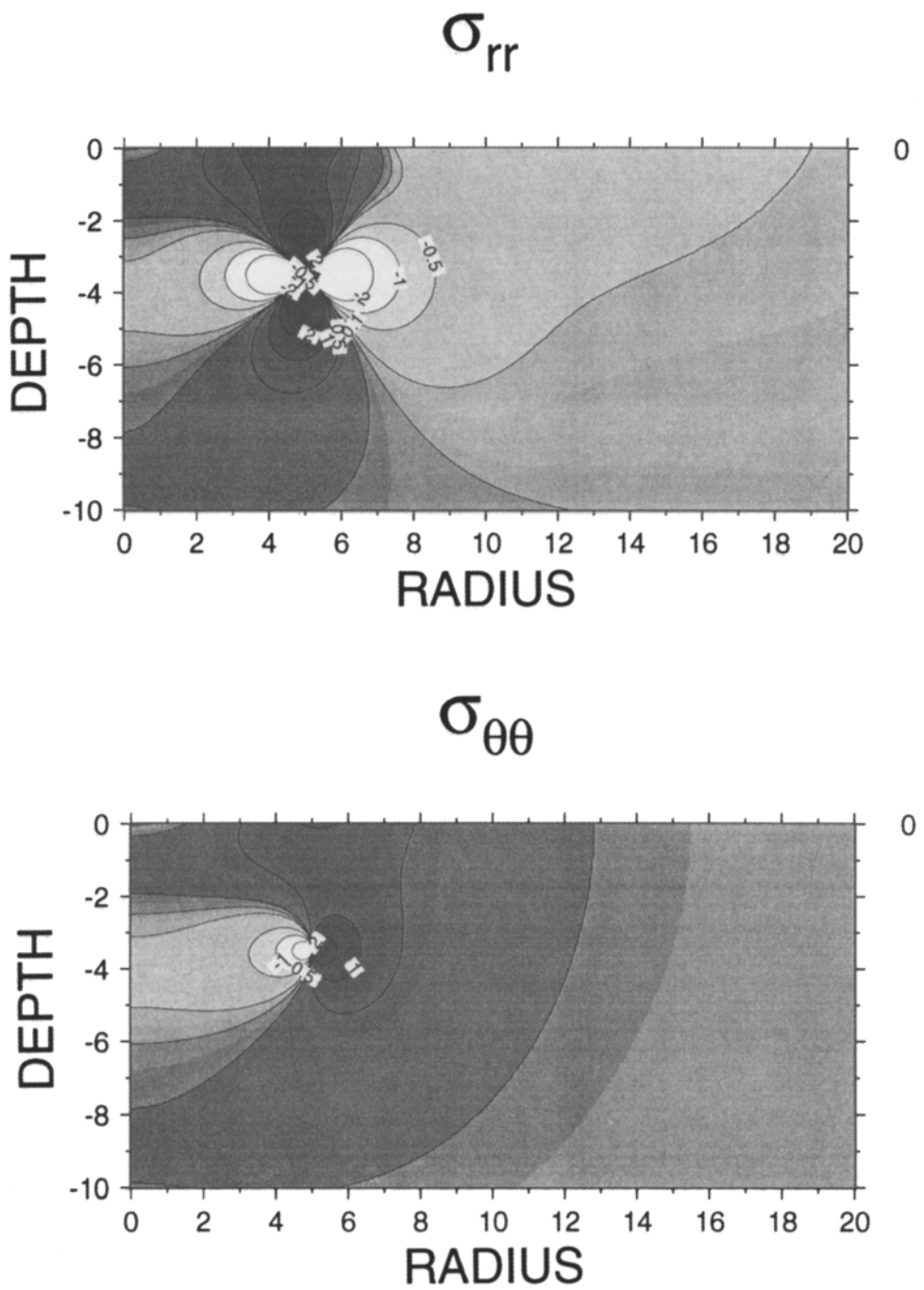

Figure 5
Stress distribution due to a change in pore pressure p at depth $d = 3.5$ and radius $\rho = 5.0$. Stresses are normalized by $10\alpha(1-2\nu)p/2(1-\nu)$. (a) σ_{rr}. (b) $\sigma_{\theta\theta}$.

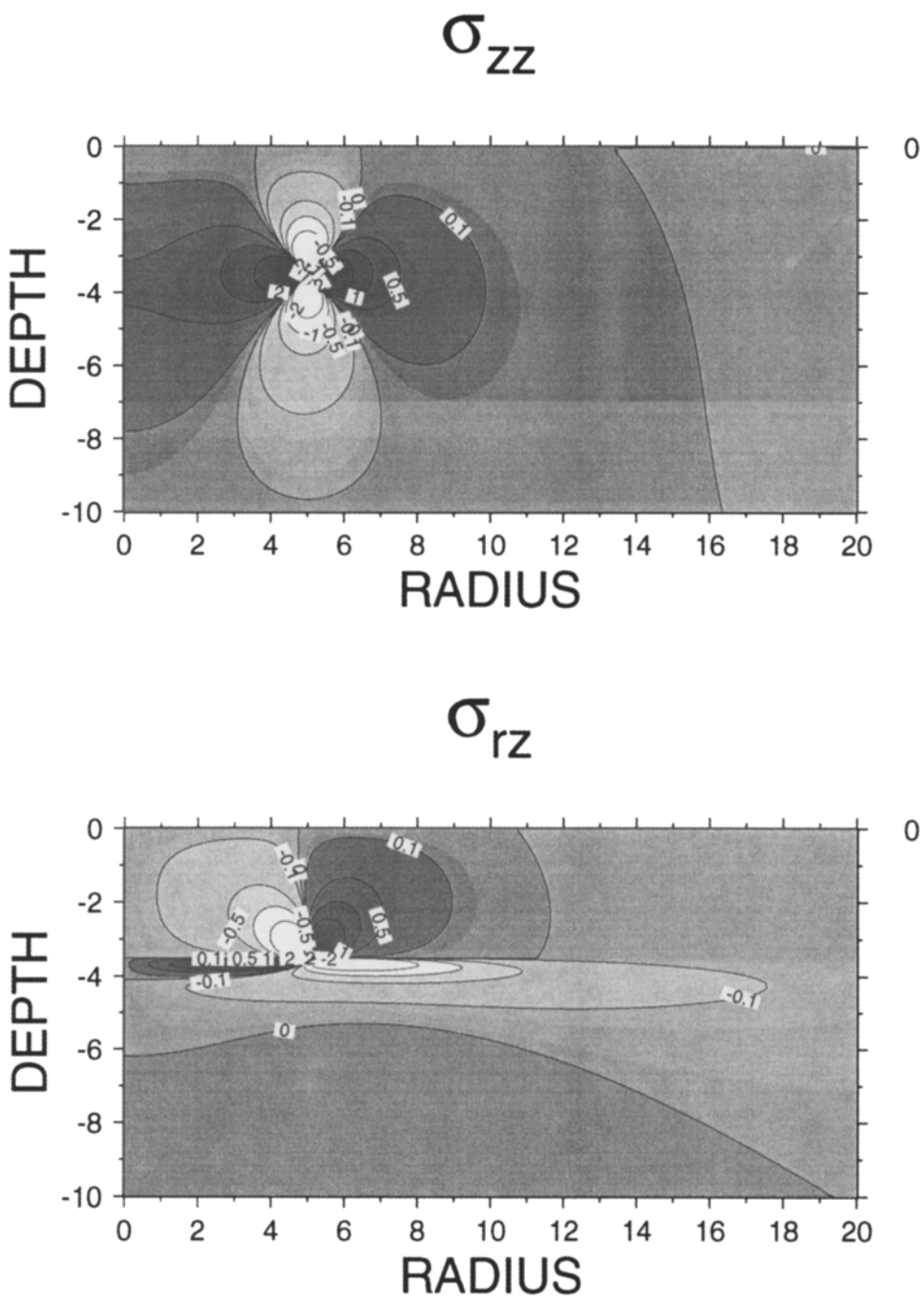

Figure 6
Stress distribution due to a change in pore pressure p at depth $d = 3.5$ and radius $\rho = 5.0$. Stresses are normalized by $10\alpha(1-2\nu)p/2(1-\nu)$. (a) σ_{zz}. (b) σ_{rz}.

$$G_{\theta\theta} = \frac{\rho}{2}\{I^{-\epsilon(z-d)}(1,0;1) + (3+4\nu)I^{(z+d)}(1,0;1) - 2zI^{(z+d)}(1,0;2)$$

$$+ I^{-\epsilon(z-d)}(1,2;1) + (3-4\nu)I^{(z+d)}(1,2;1) - 2zI^{(z+d)}(1,2;2)\} \quad (60)$$

$$G_{zz} = -\rho\{I^{-\epsilon(z-d)}(1,0;1) - I^{(z+d)}(1,0;1) - 2zI^{(z+d)}(1,0;2)\} \quad (61)$$

$$G_{rz} = \rho\{\epsilon I^{-\epsilon(z-d)}(1,1;1) - I^{(z+d)}(1,1;1) - 2zI^{(z+d)}(1,1;2)\}. \quad (62)$$

The necessary integrals are given in Appendix A following the work of EASON *et al.* (1955).

The kernels corresponding to the various stress components are shown in Figures 5 and 6, for $d = 3.5$ and $\rho = 5.0$. For a pore-pressure increase the radial stress is tensile (positive) above and below the ring, and compressive inside and outside the ring. The hoop stress, $\sigma_{\theta\theta}$ is compressive inside the ring and tensile everywhere else. The vertical stress (Figure 6) is nearly opposite to the radial stress, as expected, being compressive above and below the source and tensile in and outside the ring. Finally, the shear stress σ_{rz} is antisymmetric, with greatest magnitude above the source.

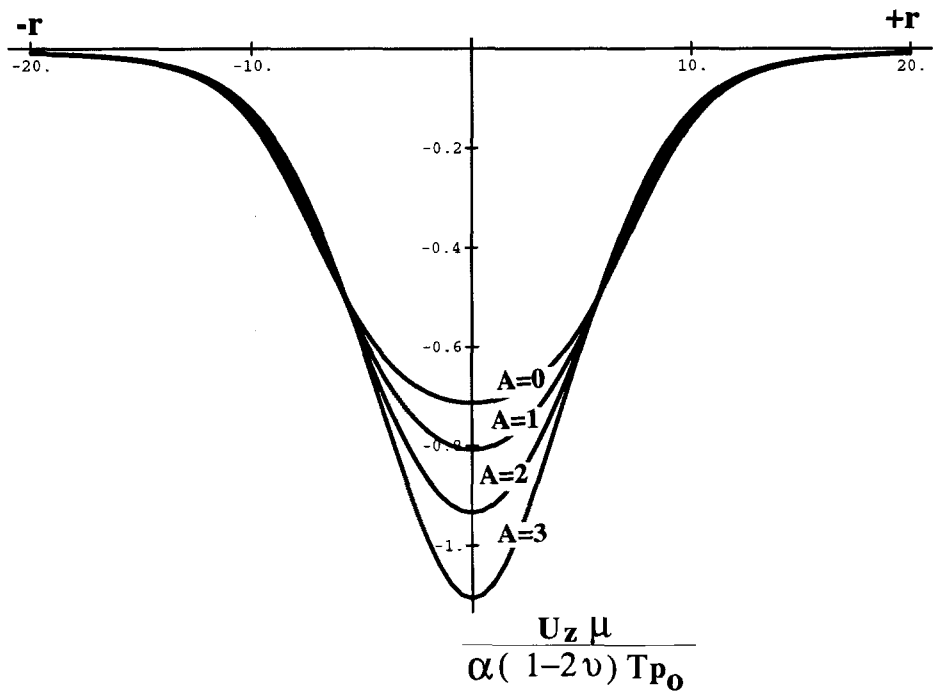

Figure 7
Predicted subsidence for reservoirs in dome structures. Reference reservoir depth $d_0 = 2.0$ km, characteristic length of reservoir pressure drop and structure $r_c = l_c = 8.0$ km. Dome amplitude $A = 0.0$, 1.0, 2.0, 3.0. p_0 maximum pressure drop; T is thickness of producing layer.

3. Examples

In this section we consider the poroelastic fields generated by distributed axisymmetric pressure reductions. The examples are chosen to simulate conditions appropriate to induced seismicity associated with hydrocarbon production. Many of the parameters are chosen to be consistent with conditions in the Lacq gas field as discussed by SEGALL *et al.* (manuscript in preparation).

As a first step we compute the surface subsidence for pressure drawdown from an axisymmetric dome-shaped reservoir. The structure is represented by a simple Gaussian shape. The depth to the reservoir layer $d(r)$ is taken to be

$$d(r) = d_0 - A[e^{-(r/l_c)^2} - \tfrac{1}{2}] \tag{63}$$

where A is the amplitude of the dome, and l_c is the characteristic length of the structure. In these calculations it is assumed that the thickness of the producing zone, T, is considerably less than the reservoir depth and the other characteristic dimensions of the reservoir.

For the purposes of computation the pressure is taken to vary with radius according to

$$p(r, t) = p_0(t)\, e^{-(r/r_c)^4} \tag{64}$$

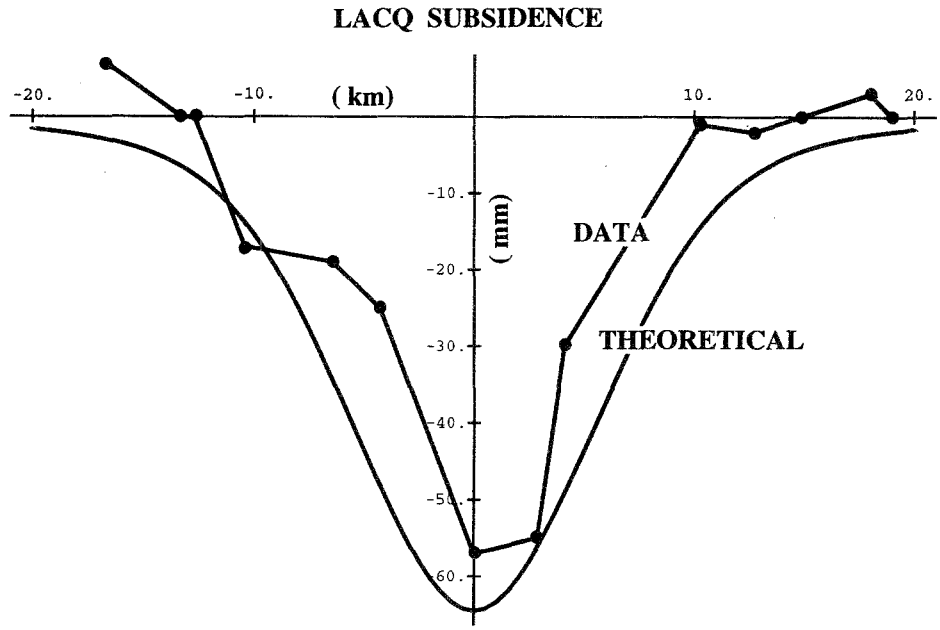

Figure 8
Comparison of predicted surface subsidence with that measured by repeated spirit leveling over the Lacq deep gas field. From SEGALL *et al.* (in preparation).

where $p_0(t)$ is the maximum pressure decline at $r = 0$, and r_c is the characteristic length of the pressure drop with radial distance.

Figure 7 shows the predicted surface displacements for $d_0 = 2.0$, $r_c = l_c = 8.0$, and a range of dome amplitudes. The maximum subsidence increases with the amplitude of the structure, while the half-width of the subsiding region is constant. Failure to account for the dome geometry could lead to a poor prediction of the ratio of maximum subsidence to half-width of the subsiding region.

If we choose material parameters appropriate for the Lacq deep gas reservoir we compute the displacements shown in Figure 8. The fit to the observed leveling data is very good, especially when one considers that the material parameters and reservoir geometry are all known independently (SEGALL *et al.*, in preparation).

I now consider the other surface observables, the radial and circumferential (hoop) strains. Figures 9 and 10 show the radial and hoop strains for a flat layer at a variety of depths. The pressure distribution is given by equation (64), with critical radius $r_c = 8.0$. Note that within the reservoir ($r < r_c$) the radial strain is negative (shortening), whereas outside the reservoir ($r > r_c$) it is positive (extend-

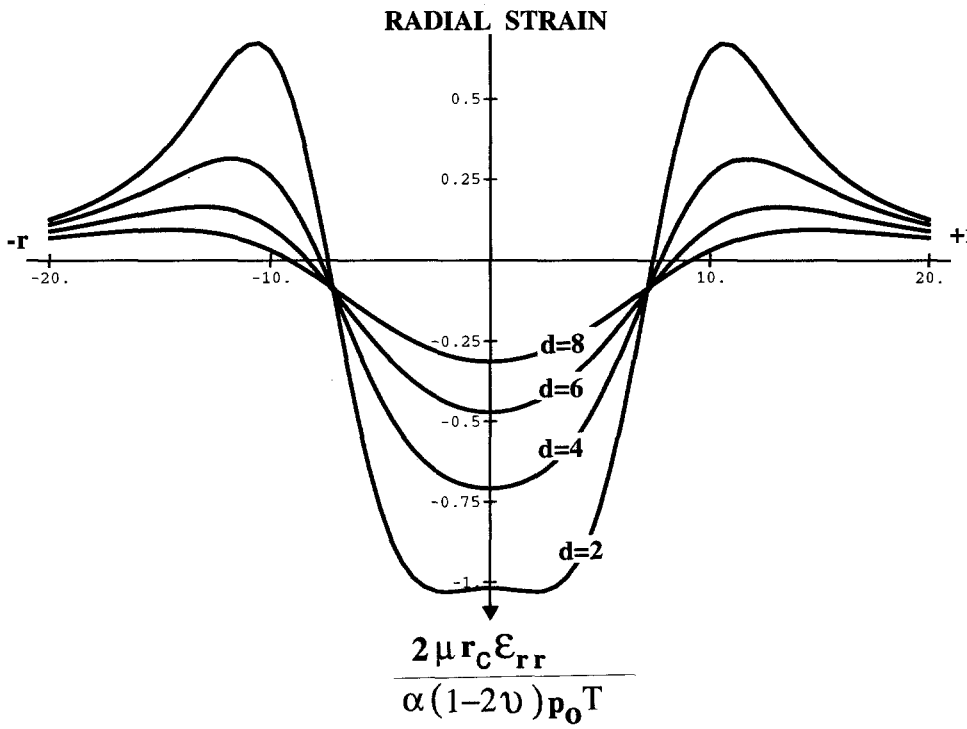

Figure 9
Surface radial strain ϵ_{rr} for a flat layer at various depths $d = 2, 4, 6, 8$. The characteristic scale of the pressure drop is $r_c = 8.0$.

ing). Because the displacements are everywhere radially inward, the hoop strain $\epsilon_{\theta\theta}$ is always negative.

The stress changes due to fluid extraction for the pressure distribution given in equation (64) are now computed. Because the pressure varies smoothly with respect to radial coordinate the stresses are everywhere finite. The radial and circumferential effective stress $\langle \sigma_{rr} \rangle$ and $\langle \sigma_{\theta\theta} \rangle$ are shown in Figure 11. The effective stress is

$$\langle \sigma_{ij} \rangle = \sigma_{ij} + \alpha p \delta_{ij} \tag{65}$$

so that $\langle \sigma_{ij} \rangle$ is given by the integral term in equation (57).

The radial stress change is compressive above and below the producing zone and is generally tensile for $r > r_c$. This is consistent with the observation that extraction induced earthquakes often exhibit thrust mechanisms above and below the reservoir, while normal faulting events are observed at the flanks of producing zones (SEGALL, 1989). If we plot the total stress, rather than the effective stress, there is a large tension, of magnitude $\alpha p(r)$, within the reservoir superimposed on the stress shown in Figure 11. Recall that the surrounding material resists the

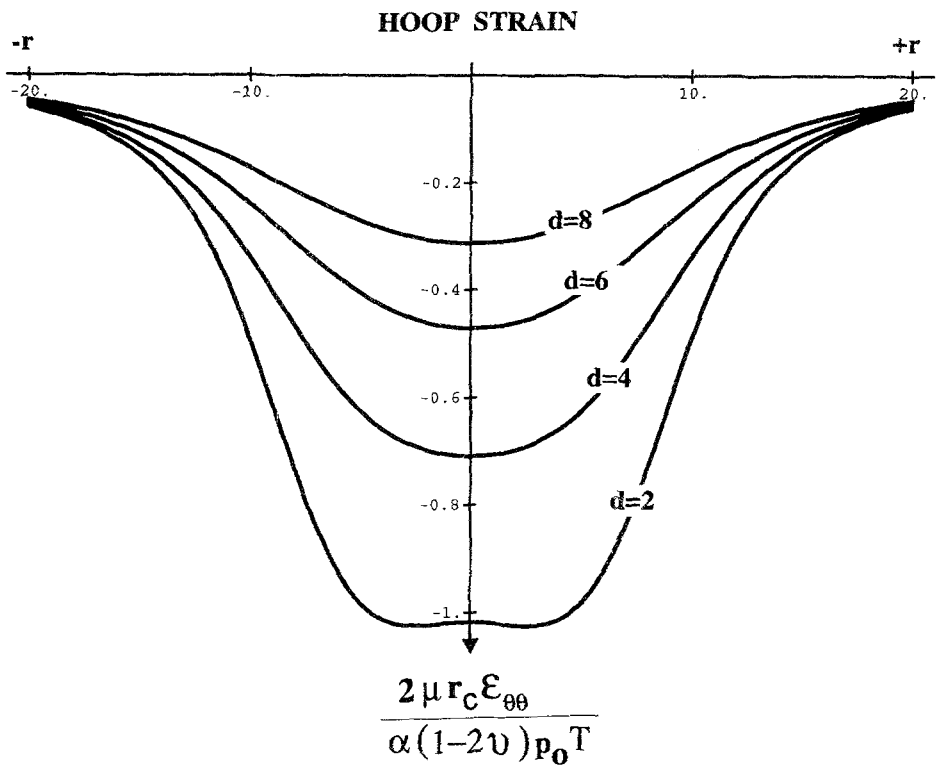

Figure 10
Surface circumferential (hoop) strain $\epsilon_{\theta\theta}$ for a flat layer at various depths $d = 2, 4, 6, 8$. The characteristic scale of the pressure drop is $r_c = 8.0$.

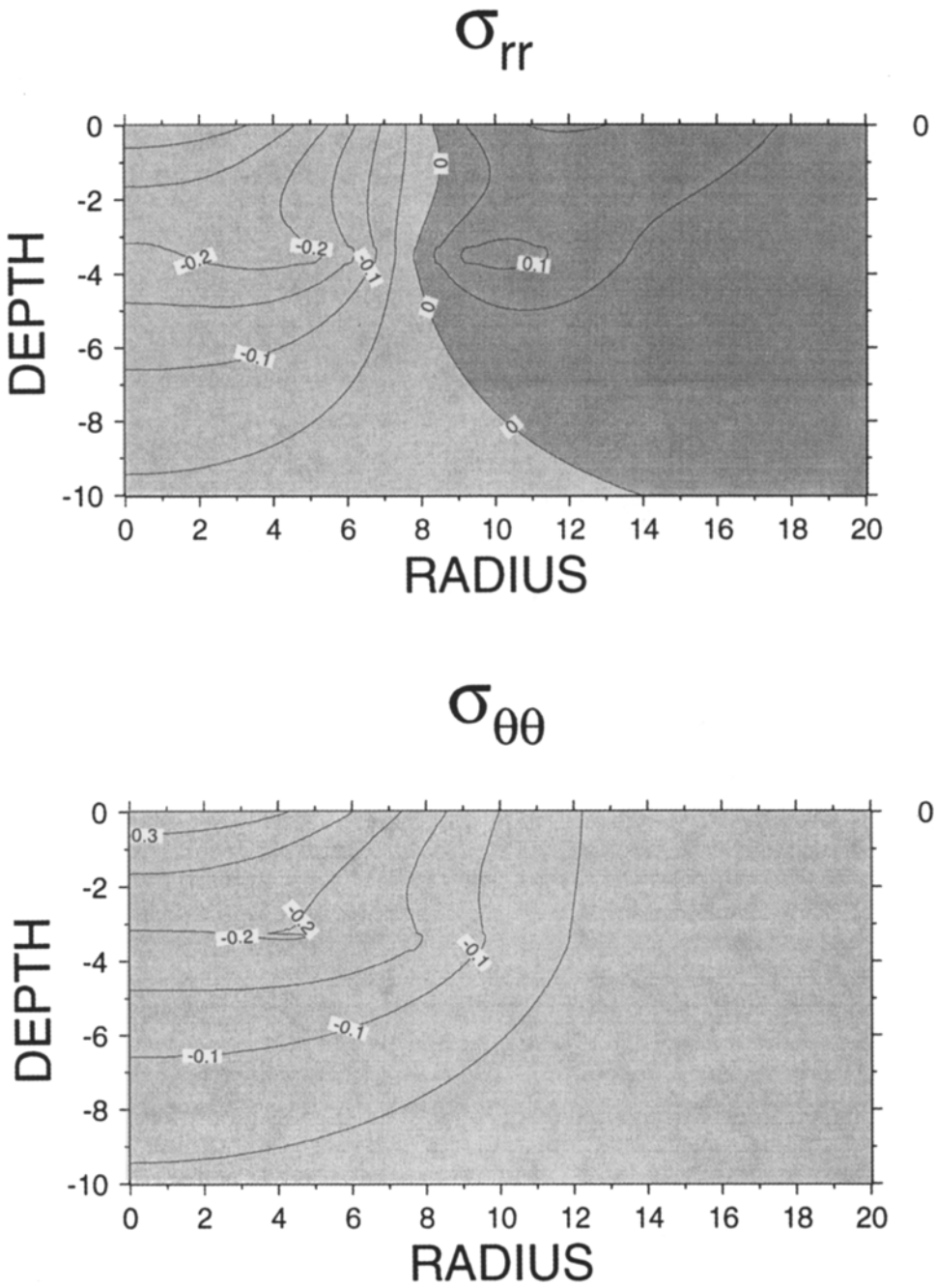

Figure 11

Effective normal stresses $\langle \sigma_{rr} \rangle$ and $\langle \sigma_{\theta\theta} \rangle$ resulting from distributed pore-pressure reduction in a flat reservoir. Peak pore-pressure change is 55 MPa; shear modulus is 19.5 GPa. Reservoir depth is 3.5 km, radius 8.0 km, and thickness 300 m. $\nu = 0.25$ and $\alpha = 0.25$. Units are MPa.

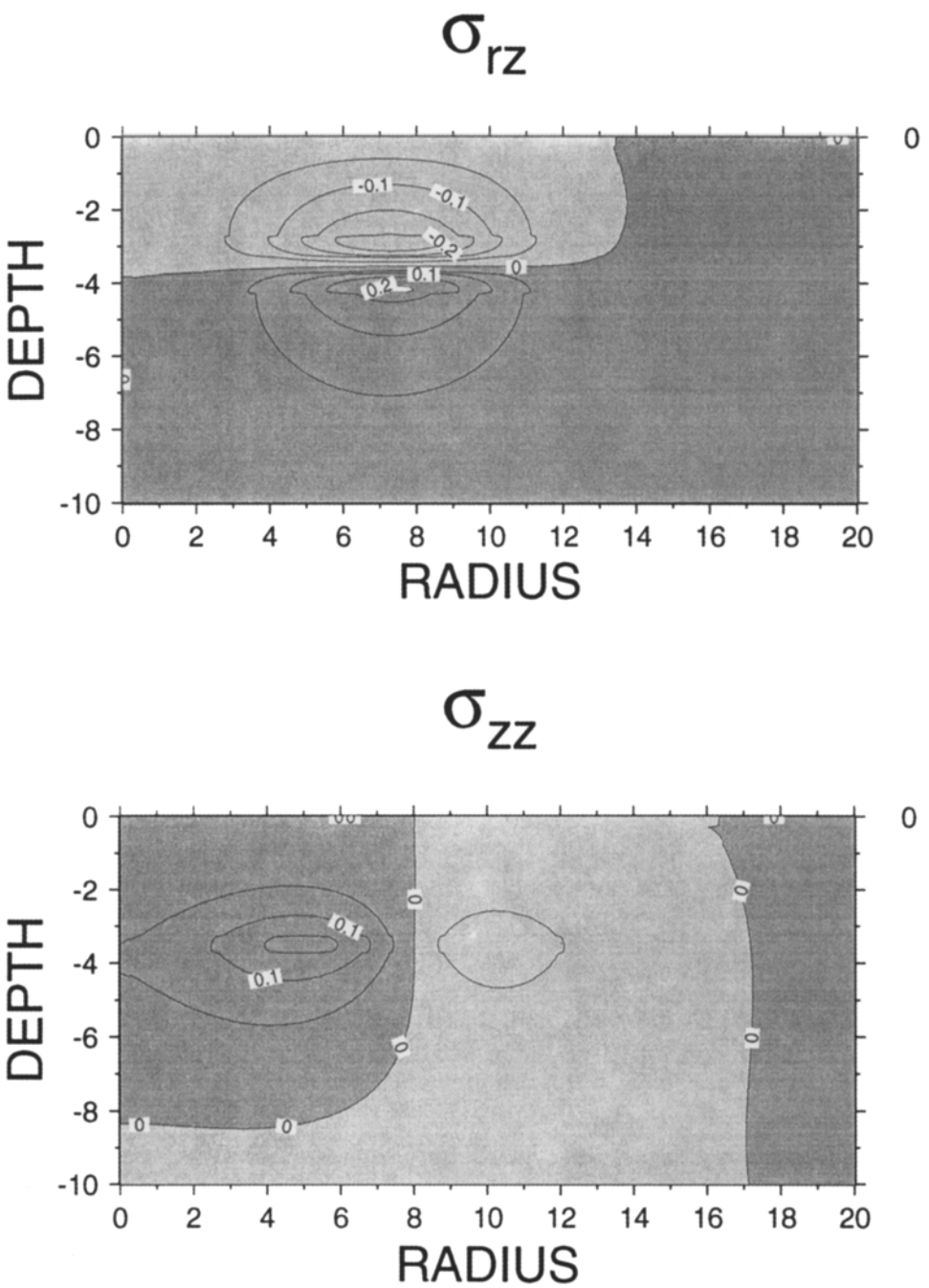

Figure 12

Shear stress $\langle \sigma_{rz} \rangle$ and effective vertical normal stress $\langle \sigma_{zz} \rangle$ resulting from distributed pore-pressure reduction in a flat reservoir. Peak pore-pressure change is 55 MPa; shear modulus is 19.5 GPa. Reservoir depth is 3.5 km, radius 8.0 km, and thickness 300 m. $\nu = 0.25$ and $\alpha = 0.25$. Units are MPa.

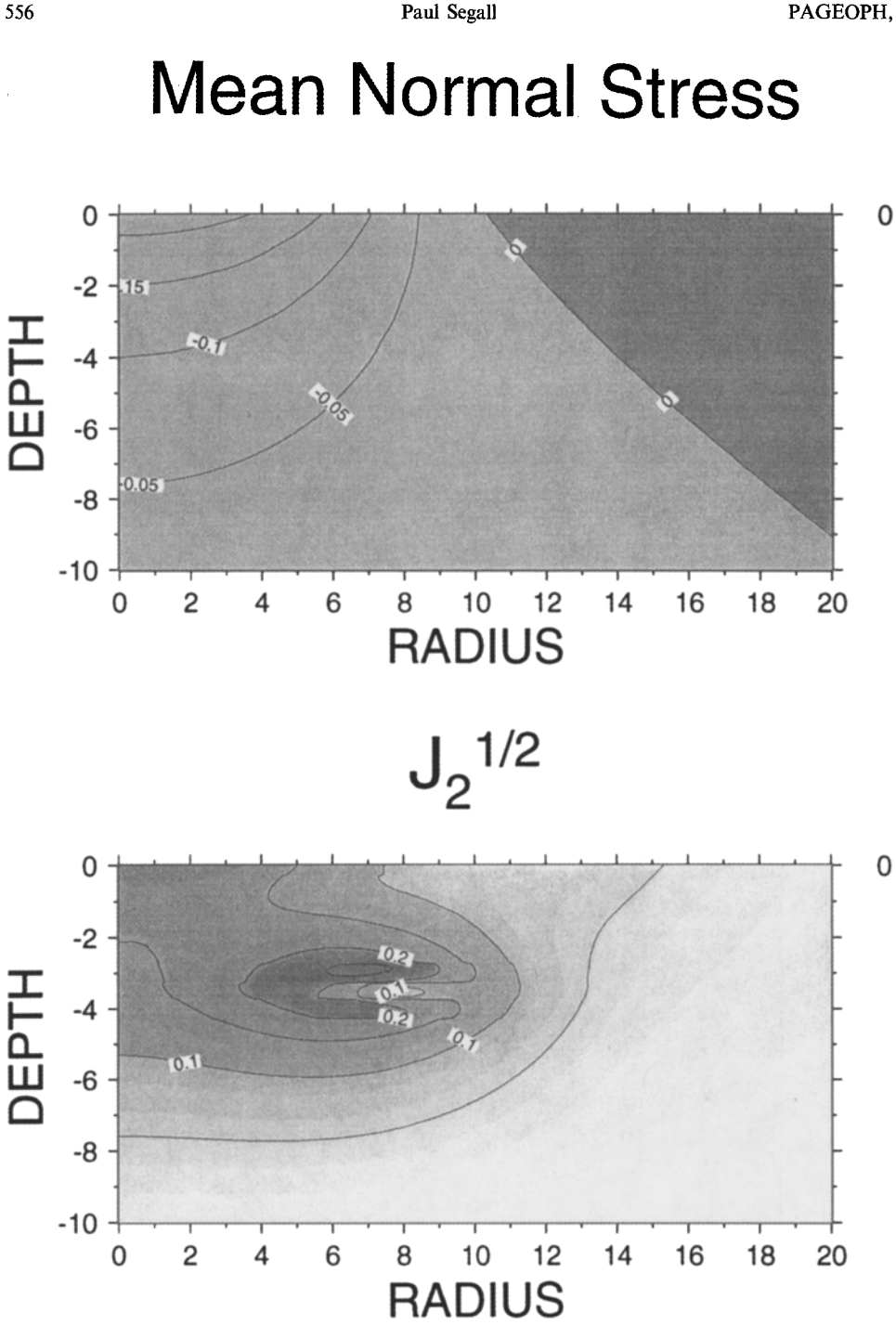

Figure 13
Stress invariants. (a) Mean normal stress $\sigma_{kk}/3$, (b) $\sqrt{J_2}$, the maximum shear. Parameters are the same as in the previous figure.

contraction of the reservoir rocks, causing the reservoir to be driven into tension. The horizontal displacements are everywhere radially inward, and this causes the hoop to be compressive everywhere (Figure 11b).

The shear stress $\langle \sigma_{rz} \rangle$ and the effective vertical normal stress $\langle \sigma_{zz} \rangle$ are shown in Figure 12. The shear stress is generally concentrated near the edge of the reservoir, $r = 8$ and $z = 3.5$ in this example. Note also that the shear stress changes sign about the plane of the reservoir. The sign of the shear is such that high angle normal faults would tend to down drop the central region with respect to the flanking zone.

Finally, the first two stress invariants are shown in Figure 13. The mean normal stress is compressive in the central region and is slightly tensile on the flanks of the reservoir. Note that since the mean stress results only from image terms there is no stress concentration near the reservoir. Again, if we plot the total stress, as compared to the effective stress, there is a large tension within the reservoir superimposed on the field shown in Figure 13. The maximum shear stress, $\sqrt{J_2}$, is strongly concentrated near the reservoir, and in particular near the edge of the reservoir (8 km in this example). If the prior stress is spatially uniform the model thus predicts that seismicity would be concentrated near the margin of the reservoir, at depths both above and below the reservoir. This is at least qualitatively consistent with the observations summarized by SEGALL (1989).

4. Discussion

The good agreement between the predicted vertical displacements and the leveling data from the Lacq field (Figure 8) supports the model explored here. In particular, the fit between observation and theory suggests that the stress changes calculated using the observed reservoir pressure changes and laboratory derived material properties should be reasonably accurate. The magnitudes of these perturbing stresses are on the order of a few tenths of one MPa (Figure 13). These changes are less than typical earthquake stress drops and markedly smaller than the expected frictional strengths of rock at modest depths. This suggests that extraction of pore fluids destabilizes faults that are already near frictional equilibrium.

There may be other factors that serve to concentrate stress above the values computed here. For example, steep gradients in pore pressure would lead to local stress concentrations. Even so, it is worth noting that the stress perturbations resulting from fluid extraction are of the same order of magnitude as fault stability changes associated with the filling of surface water reservoirs. ROELOFFS (1988) found at Lake Mead that the net effect of reservoir loading was to destabilize faults by on the order of 0.05 MPa. At Lake Mead seismicity appears to correlate with seasonal fluctuations in water height. The stress changes due to fluctuations in water level are on the order of 0.01 MPa.

In summary, observations and theory indicate that earthquakes can be induced, either by filling of surface reservoirs or by extraction of pore fluid from subsurface oil and gas fields, by equivalent changes in stress of the order of a few tenths of one MPa.

5. Acknowledgements

Much of this work was completed while I was a visiting Associate Professor at the Laboratoire Geophysique Interne et Tectonophysique of the University of Grenoble. I would like to thank the Director, G. Poupinet and J. R. Grasso for their hospitality. I also thank J. Rudnicki and D. McTigue for numerous insights into poroelasticity and to B. Segall for discussions on potential theory. The manuscript was reviewed by E. Roeloffs and P. Hsieh. This research was supported by the D.O.E. Office of Basic Energy Sciences.

6. Appendix

Here we give the integrals needed to compute stresses. I follow the notation of EASON *et al.* (1955). Let

$$I(n, m; t) = \int_0^\infty J_n(k\rho) J_m(kr) k^t e^{-ck}\, dk. \tag{66}$$

The integrals that are needed are $I(1, 0; 1)$, $I(1, 0; 2)$, $I(1, 2; 1)$, $I(1, 2; 2)$, $I(1, 1; 1)$, and $(1, 1; 2)$. Of the six integrals $I(1, 0; 1)$ and $I(1, 1; 1)$ are given by EASON *et al.* (1955) as

$$I(1, 0; 1) = \frac{\kappa^3(r^2 - \rho^2 - c^2)E(\kappa)}{8\pi r(1-\kappa^2)(\rho r)^{3/2}} + \frac{\kappa F(\kappa)}{2\pi r\sqrt{\rho r}} \tag{67}$$

$$I(1, 1; 1) = \frac{c\kappa}{2\pi(r\rho)^{3/2}} \{(1 - \tfrac{1}{2}\kappa^2)(1-\kappa^2)^{-1}E(\kappa) - F(\kappa)\} \tag{68}$$

where $F(\kappa)$ and $E(\kappa)$ are the complete elliptic integrals of the first and second kind, respectively, and $\kappa^2 = 4r\rho/(\rho + r)^2 + d^2$.

$I(1, 2; 1)$ and $I(1, 2; 2)$ are given by recursion relations in terms of elementary forms. Specifically,

$$I(1, 2; 1) = \frac{2}{\rho} I(1, 1; 0) - I(1, 0; 1) \tag{69}$$

and

$$I(1, 2; 2) = \frac{2}{\rho} I(1, 1; 1) - I(1, 0; 2). \tag{70}$$

The integral $I(1, 1; 0)$ is also given by EASON *et al.* (1955) as

$$I(1, 1; 0) = \frac{2}{\pi\kappa\sqrt{r\rho}}\{(1 - \tfrac{1}{2}\kappa^2)F(\kappa) - E(\kappa)\}. \tag{71}$$

The remaining two integrals $I(1, 0; 2)$ and $I(1, 1; 2)$ are given by differential recursion relations. Specifically,

$$I(1, 0; 2) = -\frac{\partial}{\partial c} I(1, 0; 1) \tag{72}$$

which yields

$$I(1, 0; 2) = \frac{c\kappa^3}{8\pi r(1 - \kappa^2)(r\rho)^{3/2}} \times \left\{3E(\kappa) + \frac{\kappa^2(r^2 - \rho^2 - c^2)}{r\rho}\left[\frac{(1 - \frac{1}{2}\kappa^2)E(\kappa)}{(1 - \kappa^2)} - \tfrac{1}{4}F(\kappa)\right]\right\}. \tag{73}$$

Similarly,

$$I(1, 1; 2) = -\frac{\partial}{\partial c} I(1, 1; 1) \tag{74}$$

which yields

$$I(1, 1; 2) = -\frac{1}{c} I(1, 1; 1) + \frac{c^2\kappa^3}{8\pi(1 - \kappa^2)(r\rho)^{5/2}} \times \left\{\frac{[1 - \kappa^2(1 - \kappa^2)]E(\kappa)}{(1 - \kappa^2)} - (1 - \tfrac{1}{2}\kappa^2)F(\kappa)\right\}. \tag{75}$$

REFERENCES

BIOT, M. A. (1941), *General Theory of 3-dimensional Consolidation*, J. Appl. Phys. *12*, 155–164.

DOSER, D. I., BAKER, M. R., and MASON, D. B. (1991), *Seismicity in the War-Wink Gas Field, Delaware Basin, West Texas, and its Relationship to Petroleum Production*, Bull. Seismol. Soc. Am. *81*, 971–986.

EASON, G., NOBLE, B., and SNEDDON, I. N. (1955), *On Certain Integrals of Lipschitz-Hankel Type Involving Products of Bessel Functions*, Phil. Trans. Royal Soc. London A*247*, 529–551.

GEERTSMA, J. (1973), *Land Subsidence above Compacting Oil and Gas Reservoirs*, J. Pet. Tech. *25*, 734–744.

GOODIER, J. N. (1937), *On the Integration of the Thermoelastic Equations*, Phil. Mag. *7*, 1017–1032.

GRASSO, J. R., and WITTLINGER, G. (1990), *10 Years of Seismic Monitoring over a Gas Field Area*, Bull. Seismol. Soc. Am. *80*, 450–473.

HEALY, J. H., RUBEY, W. W., GRIGGS, D. T., and RALEIGH, C. B. (1968), *The Denver Earthquakes*, Science *161*, 1301–1310.

HSIEH, P. A., and BREDEHOEFT, J. D. (1981), *A Reservoir Analysis of the Denver Earthquakes: A Case Study of Induced Seismicity*, J. Geophys. Res. *86*, 903–920.

JACKSON, J. D., *Classical Electrodynamics* (John Wiley and Sons, New York 1962).

KOCH, T. W. (1933), *Analysis and Effects of Current Movements on an Active Fault in the Buena Vista Hills Oil Field, Kern County, California*, Bull. Am. Assoc. Pet. Geol. *17*, 694–712.

KOSLOFF, D., SCOTT, R. F., and SCRANTON, J. (1980a), *Finite Element Simulation of Wilmington Oil Field Subsidence: I. Linear Modeling*, Tectonophysics *65*, 339–368.

KOSLOFF, D., SCOTT, R. F., and SCRANTON, J. (1980b), *Finite Element Simulation of Wilmington Oil Field Subsidence: II. Nonlinear Modeling*, Tectonophysics *65*, 159–183.

LOVE, A. E. H., *A Treatise on the Mathematical Theory of Elasticity* (Dover, New York 1944).

MINDLIN, R. D., and CHENG, D. H. (1950), *Thermoelastic Stress in the Semi-infinite Solid*, J. Appl. Phys. *21*, 931–933.

NOWACKI, W., *Thermoelasticity* (Pergamon Press, Oxford 1962).

NUR, A., and BYERLEE, J. D. (1971), *An Exact Effective Stress Law for Elastic Deformation of Rock with Fluids*, J. Geophys. Res. *76*, 6414–6419.

PENNINGTON, W. D., DAVIS, S. D., CARLSON, S. M., DUPREE, J. D., and EWING, T. E. (1986), *The Evolution of Seismic Barriers and Asperities Caused by the Depressuring of Fault Planes in Oil and Gas Fields of South Texas*, Bull. Seismol. Soc. Am. *76*, 939–948.

RALEIGH, C. B., HEALY, J. H., and BREDEHOEFT, J. D., *Faulting and crustal stress at Rangely, Colorado*. In *Flow and Fracture of Rocks* (Griggs volume) (Am. Geophys. Union Geophys. Monograph *16*, Washington, D.C. 1972) pp. 275–284.

RALEIGH, C. B., HEALY, J. H., and BREDEHOEFT, J. D. (1976), *An Experiment in Earthquake Control at Rangely, Colorado*, Science *191*, 1230–1237.

RICE, J. R., and CLEARY, M. P. (1976), *Some Basic Stress Diffusion Solutions for Fluid-saturated Elastic Porous Media with Compressible Constituents*, Rev. Geophys. and Space Phys. *14*, 227–241.

ROELOFFS, E. A. (1988), *Fault Stability Changes Induced Beneath a Reservoir with Cyclic Variations in Water Level*, J. Geophys. Res. *93*, 2107–2124.

SEGALL, P. (1985), *Stress and Subsidence Resulting from Subsurface Fluid Withdrawal in the Epicentral Region of the 1983 Coalinga Earthquake*, J. Geophys. Res. *90*, 6801–6816.

SEGALL, P. (1989), *Earthquakes Triggered by Fluid Extraction*, Geology *17*, 942–946.

SMITH, D. J. (1988), *Project Management of Subsidence and Ekofisk Jacking Project*, 20th Annual Offshore Technology Conference, pp. 341–358.

SULAK, R. M., and DANIELSON, J. (1988), *Reservoir Aspects of Ekofisk Subsidence*, 20th Annual Offshore Technology Conference, pp. 9–30.

WESTMILLER, R. J. (1986), *Earthquakes near Rocky Mountain House, Alberta and their Relationship to Gas Production*, Canadian J. Earth Sciences *23*, 172–181.

YERKES, R. F., and CASTLE, R. O. (1970), *Surface Deformation Associated with Oil and Gas Field Operations in the United States*, Land Subsidence, volume 1 (Int. Assoc. Sci. Hydrol., UNESCO Publication 89, 1970) pp. 55–66.

YERKES, R. F., and CASTLE, R. O. (1976), *Seismicity and Faulting Attributable to Fluid Extraction*, Engineering Geology *10*, 151–167.

(Received October 30, 1992, revised January 10, 1993, accepted January 12, 1993)